Intelligent Navigation and Micro-Spectrometer Content Inspection System for a Homecare Mobile Robot

Min-Fan Ricky Lee, Fu-Hsin Steven Chiu, Clarence W. de Silva, and Chia-Yu Amy Shih

Abstract

Homecare automation draws increasing attention due to the ageing situation. Robotic assistance allows the elderly and the disabled to live at home safely and comfortably rather than in a costly and unfamiliar healthcare facility. A hierarchical robotic assistance system is proposed that incorporates intelligent navigation and identification of the unknown medicines. ANN (Artificial Neural Network) classify the environment for selection of FLC (Fuzzy Logic Controller) based navigation strategy. The onboard micro-spectrometer senses the contents of chemical specimens. The novel histogram analysis on the transmittance and absorbance spectra is fused to recognize the nominal specimen. The proposed micro-spectrometer based content inspection system using mobile robot is also the 1st approach in the world that aimed to the home care application. The experiment demonstrates that the navigation system is robust under various uncertainties to enable the robot effectively and efficiently traverse through various environments. The on-board micro-spectrometer medicine identification system successfully classifies various nominal specimens.

Keywords: Artificial neural networks, autonomous mobile robot, fuzzy logic control, homecare robotics, micro-spectrometer.

1. Introduction

United Nation projected 22% of the global population will be 60 or older by 2050 [1]. The global aging will drastically increase health-care facility costs. World Health Organization estimated that over 1 billion people are living with some form of disability [2]. Some 110 million to 190 million people live with significant disabilities. To ensure people to live self-determined and safe in home, an acoustic monitoring system for evaluation of acoustic cues is presented [3] or detect a fall, heart attack or stroke by a smart elderly home monitoring system [4]. D. Kim et al [5] applied ANN to recognize the environment for further selection of the suitable FLC navigation strategy.

This paper aimed at the robotic assistance at home for elderly and disabled people. An integrated system is developed to navigate a mobile robot with onboard novel micro-spectrometer system to identify unknown medicines in an unstructured and unknown environment.

The analytical chemical detectors system has been designed in anticipation of a growing demand for traceable spectral measurements from sectors such as machine vision, remote sensing and color imaging [6]. The development of mobile sensor presents significant scientific and engineering challenges, such as embedded chemical agent monitor onto a robot to discover various chemicals [7], a heuristic fuzzy Kohonen clustering network navigation method is developed for an omnidirectional mobile platform [8].

A novel MEMS based micros-spectrometer is designed and fabricated from the same research group [9] and is integrated with the mobile robot proposed in this paper to identify various unknown medicines. In [10], the assembly and alignment of a micro-spectrometer constructed from discrete micro-components for the application of measuring chemical compositions and environmental applications by detecting material dependent absorption of wavelength.

X. Li et al. [11] simulated a mobile robot control strategy based on ultrasonic sensor information by combining a genetic algorithm with FLC to avoid obstacles efficiently and reach the goal quickly under multiple obstacles in the environment. C. Chen [12] simulated a neuro-fuzzy reactive navigation strategy of collision-free motion in an unknown environment with obstacles. ANNs have been applied to control a mobile robot for navigation through a maze with arbitrary obstacles [13-16]. However, the system may exhibit unstable be-

Corresponding Author: Min-Fan Ricky Lee is with the Graduate Institute of Automation and Control, National Taiwan University of Science and Technology, Taipei, Taiwan.
E-mail: rickylee@mail.ntust.edu.tw
Fu-Hsin Steven Chiu is with the Graduate Institute of Automation and Control, National Taiwan University of Science and Technology, E-mail: D9812005@mail.ntust.edu.tw
Clarence W. de Silva is with the Department of Mechanical Engineering, University of British Columbia, Canada, E-mail: desilva@mech.ubc.ca
Chia-Yu Amy Shih is with the Graduate Institute of Automation and Control, National Taiwan University of Science and Technology, E-mail: she90122@gmail.com
Manuscript received 17 April 2014; accepted 10 June 2014.

havior [17].

An indoor visual servo system for navigating the ground mobile robot was developed [18]. A fixed ceiling camera was used for the global mapping, localization and path planning of the ground mobile robot. It suffers from a stationary and fixed camera configuration.

A target tracking and following mobile robot were developed [19]. The whole-field vision system scans and locks the pose of the moving target and commands the tracking robot to follow it while avoiding obstacles.

Traditional home care robotic system focus on operating in structured and certain environment, wheelchair-mounted and stationary video monitoring. Few of them address the integration of autonomous navigation and onsite medicine identification. This paper develops an autonomous mobile robot system to facilitate healthcare services for the elderly and disabled. The literatures reviewed so far suffer from

- Only simulation conducted without experimental validation in an actual robot,
- Only kinematic model is applied without considering dynamics [20, 21],
- Aimed at simple setup and specific situation of the terrain or environment,
- Single sensor was used for range measurement [22],
- Centralized architecture, payload increased and difficult to maintain,
- Partial sensor installed in the environment,
- The medicine identification system was not on robot for on-site analysis.

To overcome these problems, this paper proposes an intelligent navigation and micro-spectrometer content inspection system for a homecare mobile robot. The significance of this work is summarized as follows:

- Novelty, According to the literature reviewed, our approach is the world 2nd mobile robot integrated with the micro-spectrometer for remote sensing of the environment (the 1st one is the Curiosity Rover in Mars by NASA, USA)
- Portability, The micro-spectrometer is designed and fabricated by the same group that is the world smallest micro-spectrometer.
- Real-time, On-site unknown chemical content analysis in the homecare environment (i.e. medicine).
- Less Costly, Autonomous sampling of specimen by manipulator on mobile robot (i.e. human care taker).
- Efficiency and Accuracy, Automatic pattern recognition of the existence and concentration of the sample specimen.
- Autonomous, Autonomous navigation and remote sensing/perception of the bottle content in the home care environment.
- The operation is decentralized, reduce the computer loading on the robot and easy to maintain.

2. Method

This paper focuses on developing the intelligent navigation of a mobile robot and specimen sensing/perception as shown in Figure 1. The alignment control will be presented in a separate paper.

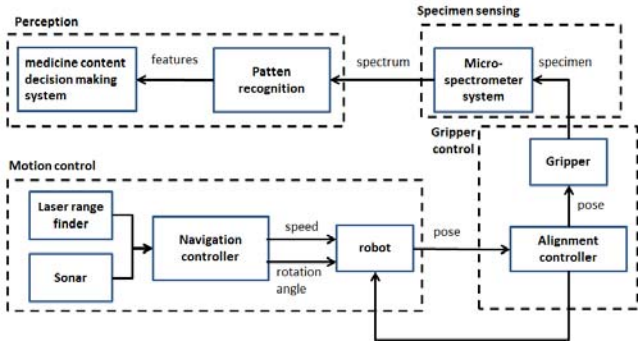

Figure 1. System architecture.

Figure 2 and Figure 3 shows the proposed hierarchical and decentralized system. The high-level controller receives the sensory measurements (ranges) from the low-level control system in the mobile robot. The reasoning mechanism of the intelligent controller makes a control decision (velocity and steering angle) and transmitted to the low-level control system. IEEE 802.11 b/g is used as the wireless communication protocol.

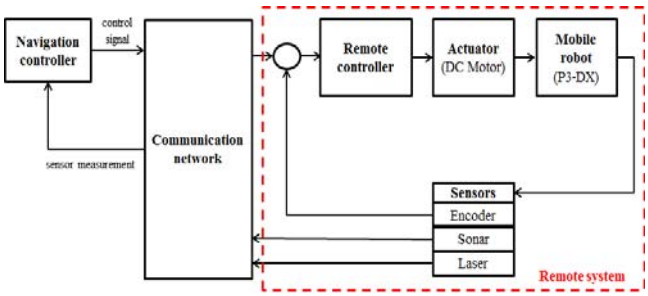

Figure 2. Hierarchical networked control system.

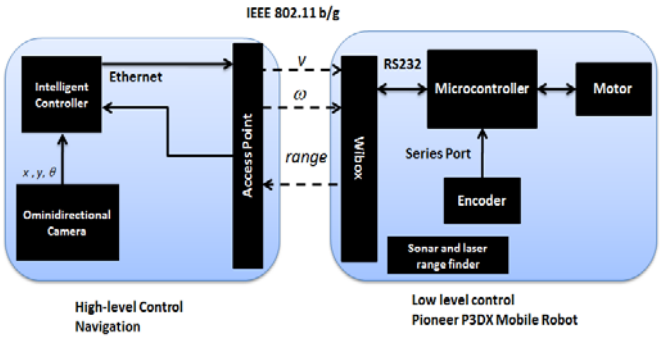

Figure 3. System layout.

Figure 4 shows the flow chart of the proposed system. ANN is adopted as environment classifier to select cor-

responding FLC for motion control. The spectrum of an unknown specimen is further acquired via onboard micro-spectrometer upon robot's arrival of the target site. The histogram of the spectrum distribution is computed for classification of the specimen.

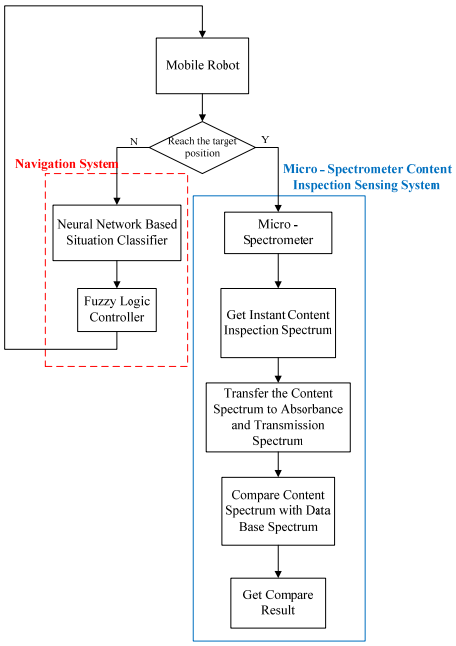

Figure 4. System architecture.

A. *ANN environment classifier*

The range signals from eight sonars as shown in Figure 5 are fed into the ANN as the training data pattern

$$x_i = \begin{cases} 0, & S_i \in [0\ cm \quad 50\ cm] \\ 1, & S_i \in [50\ cm \quad 100\ cm] \\ 2, & S_i \in [100\ cm \quad \infty] \end{cases} \qquad (1)$$

where

S_i Range measurements from sonars, i =1 to 8

x_i Input to the ANN, i =1 to 8

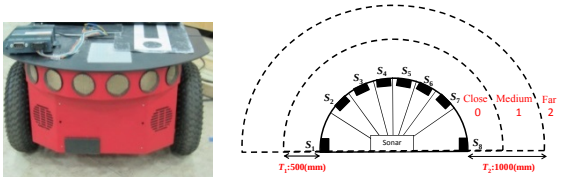

Figure 5. Sonars arrangement: (Left) in mobile robot; (Right) defined configuration.

To reduce the computation, only 28 out of 3^8 possible training patterns are adopted to classify six environment patterns as shown in Figure 6. For example, if an obstacle is positioned as left wall (t_1=1), the corresponding input is [0 1 2 2 2 2 2 2].

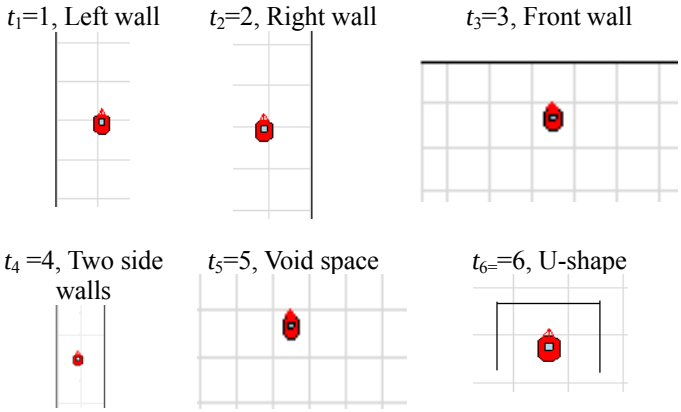

Figure 6. Classifications of the surrounding environment.

Figure 7 shows the proposed ANN structure with one input layer (8 nodes [x_1 … x_8]), three hidden layers (20, 10 and 5 nodes, respectively) and one output layer (1 nodes t_i).

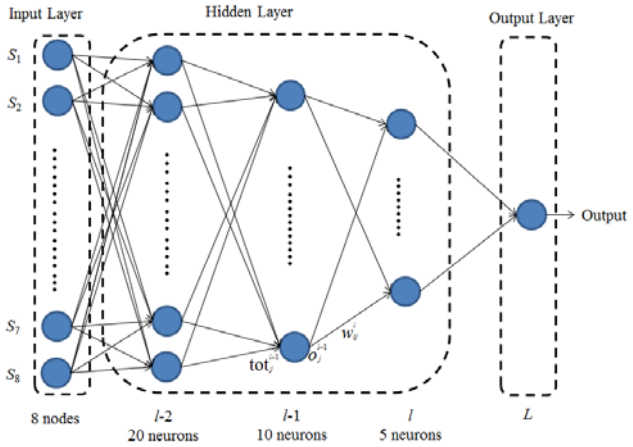

Figure 7. The ANN used as situation classifier.

Back propagation is used for training the ANN. The network weights are optimized to minimizes the network cumulative error $E_c(k)$ with following procedure [23].

$$E_c(k) = \sum_{k=1}^{n} E(k) = \frac{1}{2} \sum_{k=1}^{n} \sum_{i=1}^{q} [t_i(k) - o_i(k)]^2 \qquad (2)$$

1. Initialization: weights (small random values)
2. Apply input pattern: k^{th} input-output training data set $(x^{(k)}, t^{(k)})$.

$$x^{(k)} = (x_1, \cdots x_8), k = 1 \cdots 6 \qquad (3)$$

3. Forward propagation: Apply the input pattern to the ANN and compute the ANN signals from the input to the output

$$o_i^{(l)}(k) = f(\sum_{p=0}^{n_{l-1}} W_{ip}^{(l)} o_p^{(l-1)}) \qquad (4)$$

where

$$f(tot) = \frac{1}{1+e^{-\lambda \cdot tot}}, \lambda = 1 \qquad (5)$$

4. Output error measure: Compute total error E and the back-propagation error signal δ at the output layer (L):

$$E = \frac{1}{2}\sum_{i=1}^{n}(t_i - o_i^L)^2 + E \quad (6)$$

$$\delta_i^{(L)} = [t_i - o_i^L]\left[f'(tot_i^{(L)})\right] \quad (7)$$

where

$$f'(tot) = o(1-o)$$

5. Error back propagation: Propagate the errors backward to update the weights W and the error signals δ of the preceding layers for $l < L$

$$\Delta W_{ij}^{(l)} = -\eta\delta_i^{(l)}o_j^{(l-1)}, l = L, \cdots, 1 \quad (8)$$

$$\delta_i^{(l-1)} = f'(tot_i^{(l-1)})\sum_p \delta_p^{(l)} w_{pi}^{(l)} \quad (9)$$

6. Repeat steps 2 to 5 for another training data set and compute error E.
7. After using all training data sets (i.e. one epoch), if the final error E is less than a predetermined tolerance, the network has been trained. If not, repeat the process for another epoch.

The goal is to make the outputs (o) approach the targets (t) by training the weights so as to make the errors (E) approach zero.

B. *FLC motion control*

FLC is developed to control the robot for approaching the target position while avoiding the obstacles. Based on the results from the ANN classifier, two behaviors are implemented using four *Sugeno* FLC. Different inputs to FLC but the same outputs, turning angle and velocity of the robot.

- *Target steering behavior*

The 1st input d (distance between robot and target) which is measured from the onboard sonar as shown in Figure 8.

The 2nd input θ illustrated in Figure 8 is calculated by

$$\theta = \tan^{-1}\frac{y_T - y_R}{x_T - x_R} \quad (10)$$

where

x_T, y_T Position of the target measured from the ceiling camera.

x_R, y_R Current position of the robot.

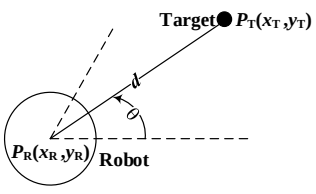

Figure 8. The angle and distance between robot and target.

Membership functions $\mu_{D_i}(d)$ consists of 3 Fuzzy sets (i=1 to 3) is applied to fuzzify the input d as shown in Figure 9 (from left to right). The corresponding fuzzy labels denote [C (Close), M (Medium), F (Far)].

$$D = \left\{\left(d, \mu_{D_i}(d)\right); d \in [0 \quad 1500], D \in [0 \quad 1]\right\} \quad (11)$$

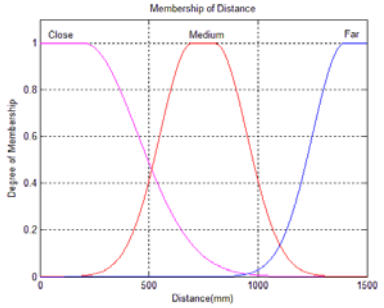

Figure 9. Input membership function: $\mu_{D_i}(d)$.

Membership functions $\mu_{\theta_i}(\theta)$ consists of 6 Fuzzy sets (i=1 to 6) is applied to fuzzify the input θ as shown in Figure 10 (from left to right). The corresponding fuzzy labels [S (Small), LS (Less Small), LM (Less Middle), M (Middle), LB (Less Big), B (Big)].

$$\theta = \left\{\left(\theta, \mu_{\theta_i}(\theta)\right); d \in [0 \quad 180], D \in [0 \quad 1]\right\} \quad (12)$$

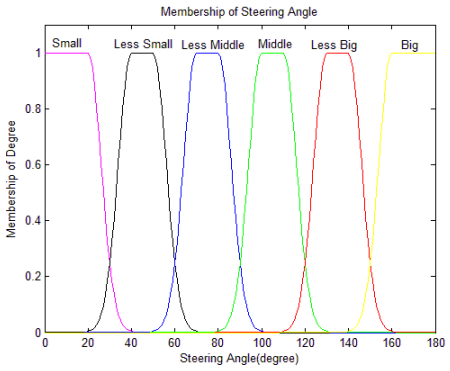

Figure 10. Input membership function: $\mu_{\theta_i}(\theta)$.

Two-sided Gaussian membership function is applied as in (13). The corresponding parameters listed in Tables 1 and 2.

$$\mu_{X_i}(x) = \begin{cases} exp\left[\frac{-(x-c_1)^2}{2(-\sigma_1)^2}\right] & if \quad x \le c_1 \\ 1 & if \quad c_1 < x < c_2 \\ exp\left[\frac{-(x-c_2)^2}{2(\sigma_2)^2}\right] & if \quad c_2 \le x \end{cases} \quad (13)$$

Table 1. FLC state parameters for the input d.

Fuzzy State	c_1	σ_1	c_2	σ_2
F	1400	150	∞	∞
M	700	150	800	150
C	0	∞	200	250

Table 2. FLC state parameter for the input θ.

Fuzzy States	c_1	σ_1	c_2	σ_2
S	∞	6	20	6
LS	40	6	50	6
LM	70	6	80	6
M	100	6	110	6
LB	130	6	140	6
B	160	6	∞	6

Takagi-Sugeno fuzzy model is used for rule evaluation as

R^i: if $f^i(x_1 \text{ is } A_1, \ldots, x_k \text{ is } A_k)$ then $y^i = g^i(x_1, \ldots, x_k)$

$$g^i(x_1, \ldots, x_k) = p_0^i + p_1^i x_1 + \cdots + p_1^i x_k \quad (14)$$

where

R^i i^{th} rule in the knowledge base.

f logical function connect the proposition in the premise (*if* part)

g consequence function (*then* part) upon the implication

x_k Input sensor measurement (e.g. range between robot and obstacle measurement from sonar)

y^i Output control action to robot (e.g. steering angle, velocity).

The minimum operator is used as in f to generate the firing strength of the i^{th} rule

$$w_i = min_j \left\{ \mu_{A_j}(x_i) \right\} \quad (15)$$

The final output is

$$\frac{\sum_{i=1}^{n} w_i y^i}{\sum_{i=1}^{n} w_i} \quad (16)$$

Case 1: Left-wall and right-wall

The applicable motion controller is illustrated in Figure 11. If the wall and the target are on the same side of the robot, the controller activates the "along-the-wall behavior" with linear velocity $V_0 = 20$ (mm/s) and turning angle $\theta = 0$ (moving straight).

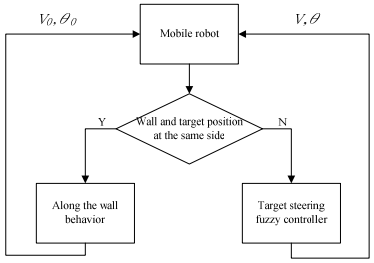

Figure 11. Motion control: left-wall or right-wall.

If the wall and the target position are on the opposite sides of each other *w.r.t.* the robot, it activates the target steering behavior. The output functions for the robot velocity (V) and turning angle (θ) are:

$$g_V(d_t) = p \times d_t + r \quad (17)$$

$$g_\theta(d_w, \theta_t) = A \times d_w + B \times \theta_t + C \quad (18)$$

where

$g_v(d_t)$ Function of output robot velocity.

d_t Distance between the robot and target.

$g_\theta(d_w, \theta_t)$ Function of robot turning angle.

d_w Distance between the wall and the robot.

θ_t Steering angle between the robot heading direction and the target.

p, r, A, B and C Parameters in the rules listed in Table 3 and 4.

Table 3. Rule base of velocity FLC.

	If	Then	
No.	d	p	r
1	C	0.002	0
2	M	0.003	0
3	F	0.004	0

Table 4. Rule base of the turning angle FLC.

	If		Then		
No.	d	θ	A	B	C
1	C,M,F	LS,S	0.0001	0.3	0
2	M	LM	0.0001	0.3	0
3	C	LM,M	0.0001	0.3	5
4	M	M	0.0001	0.3	5
5	F	LM	0.0001	0.3	5
6	C,M,F	LB,B	0.0001	0.2	10
7	F	M	0.0001	0.2	10

Case 2: Empty

The applicable control rules are summarized in Tables 5 and 6. The output functions for the robot velocity (V) and turning angle (θ).

$$g_V(d_t) = p_1^i \times d_t + p_0^i \quad (19)$$

$$g_\theta(\theta_t) = q_1^i \times \theta_t + q_0^i \quad (20)$$

Table 5. Rule base of the velocity FLC.

	If	Then	
No.	d	p_1^i	p_0^i
1	C	0.02	3
2	M	0.03	0
3	F	0.04	0

Table 6. Rule base of the turning angle FLC.

	If	Then	
No.	θ	q_1^i	q_0^i
1	S, LS	0.3	0
2	LM,M	0.3	5
3	LB,B	0.2	10

- *Target steering behavior*

The obstacle orientation is detected by the eight fixed sonars as [-90°, -50°, -30°, -10°, 10°, 30°, 50°, 90°]. The membership functions contain the subspaces defined as [*L* (Left), *FLL* (Front-Left-Left), *FFL* (Front-Front-Left), *F* (Front), *FFR* (Front-Front-Right), *FRR* (Front-Right-Right), *R* (Right)] are shown in Figure 12. The parameters in (13) are listed in Table 7.

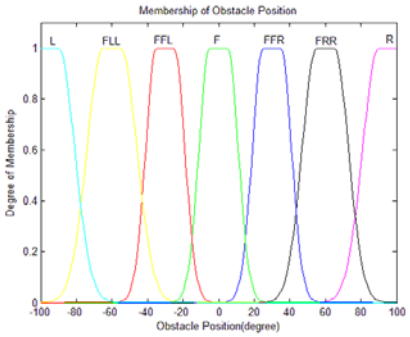

Figure 12. Membership functions for obstacle orientation.

Table 7. Fuzzy state parameters (input): obstacle orientation.

Fuzzy States	c_1	σ_1	c_2	σ_2
L	-100	100	-90	-9
FLL	-65	6	-25	-6
FFL	-35	6	-25	-6
F	-5	6	5	-6
FFR	55	8	65	-8
FRR	55	8	65	-8
R	90	9	100	-100

Case 3: Front wall and maze

For front wall, the input range is the averaged two front sonar sensors (S_4 and S_5) and obstacle orientation. For the maze, the input is the minimum of the eight front sonars (S_1 to S_8) and the obstacle orientation. The rules for the front wall and maze are listed in Table 8 to 11.

$$g_V(d_o, \theta_o) = p \times d_o + q \times \theta_o + r \quad (21)$$

$$g_\theta(d_o, \theta_o) = A \times d_o + B \times \theta_o + C \quad (22)$$

where

$g_V(d_0, \theta_0)$ Function of the output robot velocity.
d_0 Distance between the robot and obstacle.
θ_0 Obstacle orientation.
$g_\theta(d_0, \theta_0)$ Function of the robot turning angle
p, q, r, A, B and C parameters.

Table 8. Rule base of the velocity FLC: front wall.

	If		Then		
No	Distance	Obstacle Position	*p*	*q*	*r*
1	C,	L,FLL	0.05	0.04	0
2	C	FFL,F,FFR,FRR, R	0.07	0.03	-17.5
3	M,F	L,FLL, FFL,F,FFR,FRR, R	0.07	0.03	-17.5

Table 9. Rule base of the turning angle FLC: front wall.

	If		Then		
No	Distance	Obstacle Position	*p*	*q*	*r*
1	C	FLL,FRR	-0.025	-0.05	20.5
2	C	FFL,F,FFR	-0.04	-0.5	35
3	C	L,R	0	0	0
4	M,F	L,FLL, FFL,F,FFR,FRR,R	0	0	0

Table 10. Rule base of the velocity FLC: maze.

	If		Then		
No	Distance	Obstacle Position	*p*	*q*	*r*
1	C,	L,FLL,FRR,R	0.05	0.04	0
2	C	FFL,F,FFR	0.06	0.03	-20
3	M,F	L,FLL, FFL,F,FFR,FRR,R	0.06	0.03	-20

Table 11. Rule base of the turning angle FLC: maze.

	If		Then		
No	Distance	Obstacle Position	*p*	*q*	*r*
1	C	FLL,FRR	-0.025	-0.05	20.5
2	C	FFL,F,FFR	-0.04	-0.5	35
3	C	L, R	0	0	0
4	M,F	L,FLL, FFL,F,FFR,FRR,R	0	0	0

C. *Content identification system*

A micro-spectrometer-based is adopted to identify the contents of a specimen as illustrated in Figure 13. Various compounds absorb light at different wavelengths and it is used as the feature for pattern recognition.

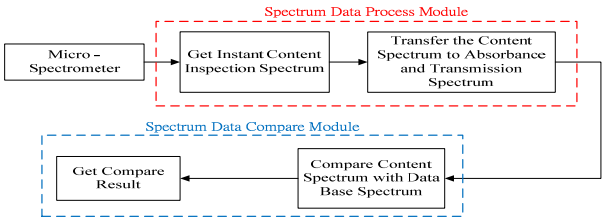

Figure 13. Micro-spectrometer based content identification.

The light source passes through the tested specimen and the spectra of *Transmittance* and *Absorbance* is measured by the micro-spectrometer as

$$T\% = {}^{I}/_{I_0} \times 100 \quad (23)$$

$$A = -log\,(T) = -log\frac{I}{I_O} \quad (24)$$

where

T Percentage of light transmitted through the specimen.
I Light energy transmitted through the specimen.
I_0 Energy transmitted through the reference specimen (water).
A Amount of light absorbed by that tested specimen.

The histogram method is used to analyze the transmittance and absorbance spectra of the tested content, as shown in Table 12 and Table 13, respectively. The results are compared with the database spectra.

Table 12. Histogram of the transmittance database spectrum.

Interval $D[m]$	Range
$D_T[0]$	If 0 $<T_i<=$ 15
$D_T[1]$	If 15 $<T_i<=$ 25
$D_T[2]$	If 25 $<T_i<=$ 35
$D_T[3]$	If 35 $<T_i<=$ 45
$D_T[4]$	If 45 $<T_i<=$ 55

Table 13. Histogram of the absorbance database spectrum.

Interval $D[m]$	Range
$D_A[0]$	If -0.75 $<A_i<=$ -0.25
$D_A[1]$	If -0.25 $<A_i<=$ 0.25
$D_A[2]$	If 0.25 $<A_i<=$ 0.75
$D_A[3]$	If 0.75 $<A_i<=$ 1

The spectra of the tested content are compared with the database spectra through upper-bound and lower-bound numbers with an adjustment parameter k as

$$P[m] = D[m] \times \left(1 + \frac{k}{100}\right) \quad (25)$$

$$N[m] = D[m] \times \left(1 - \frac{k}{100}\right) \quad (26)$$

The similarity of the transmittance spectrum histogram of the tested specimen with the sample spectrum in the database is evaluated according to:

If $N[m] \le D[m] \le P[m]$

Then *correct_ rate*= *correct_ rate*+1

$$Similarity_T = \frac{correct\_rate \times (100-k)}{5} \quad (27)$$

$$Similarity_A = \frac{correct\_rate \times (100-k)}{4} \quad (28)$$

3. Results

The mobile robot system developed is shown in Figure 14. It is two wheel differential drive with 8 forward-facing sonars. The command center communicates with the robot though a wireless network. The micro–spectrometer and the light source are attached to the gripper.

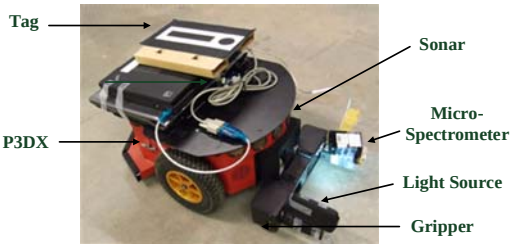

Figure 14. The prototype mobile robotic system.

The wide-angle camera mounted on the ceiling, as shown in Figure 15, captures images of the experimental environment and localizes the robot.

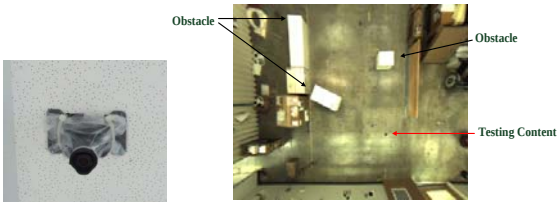

Figure 15. Experimental setup: (Left) Camera on the ceiling; (Right) Photo taken from the camera.

The uncertainty of the laser range finder is evaluated through the computed values of mean, standard deviation and relative error as

$$\bar{x} = \frac{1}{N}\sum_{i=1}^{N} x_i \quad (29)$$

$$\sigma = \sqrt{\frac{1}{N}\sum_{i=1}^{N}(x_i - \bar{x})^2} \quad (30)$$

$$\eta = \frac{x_{measure} - x_{nominal}}{x_{nominal}} \quad (31)$$

where $\bar{x}$ represent mean value, σ is Standard deviation, η is Relative error, N is Number of samples.

Table 14 summarizes the static error of the laser range finder at the three scan angles: 0°, −0.3° and +0.3°, with 100 samples at each angle (N = 100). The nominal distance is 500 mm.

Figure 16 shows the results of uncertainty in the laser range finder measurement. The relative error is 2.8% over the nominal distance 500 *mm*.

Table 14. Laser range finder uncertainty.

Angle	$\bar{x}$ (mm)	σ	η (%)
−0.3°	512.38	2.83121	2.476
0°	514.49	2.45153	2.898
+0.3	515.41	2.31854	3.082

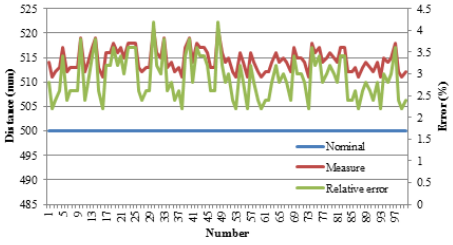

Figure 16. Uncertainty of the laser range finder.

A. *Target steering behavior*

The target steering behavior in an obstacles –free environment is tested. The robot just moves toward the target position. Figure 17 shows the setup scenario in top-view. Figure 18 (Top Left) shows the trajectory of the robot from the start S (-1176 mm, -2083 mm) to the target T (500 mm, 500 mm). The final position of the robot is (498 mm, 490 mm). Figure 18 (Top Right) shows the distance between the robot and the target. The final distance error is 10 mm. Figure 18 (Bottom Left) shows the velocity of the robot. Figure 18 (Bottom Right) shows the turning angle of the robot.

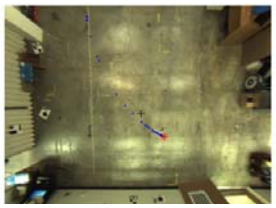

Figure 17. Top-view and trajectory of the robot.

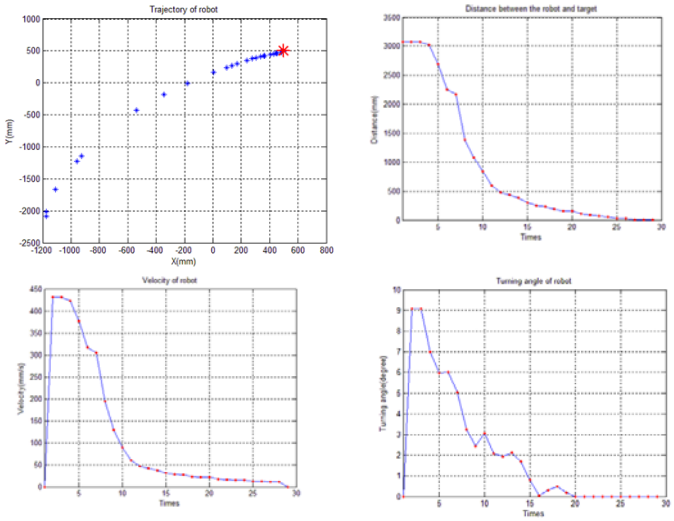

Figure 18. (Top Left) trajectory of the robot; (Top Right) Distance between the robot and target; (Bottom Left) Velocity of the robot; (Bottom Right) Turning angle of the robot.

B. *Obstacle avoidance behavior*

The obstacle avoidance behavior of the robot is evaluated. The robot does not seek the goal location while avoiding the obstacles. Figure 19 shows the maze setup scenario and the robot trajectory.

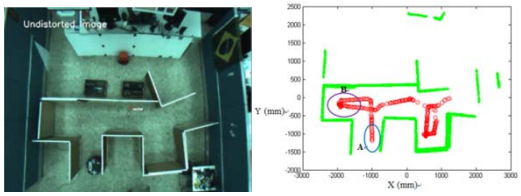

Figure 19. (Left) Maze; (Right) Trajectory of the robot.

Figure 20 shows the current orientation of the obstacle w.r.t. the robot, the distance between the closest obstacle and the robot, the velocity of the robot, and the turning angle of the robot.

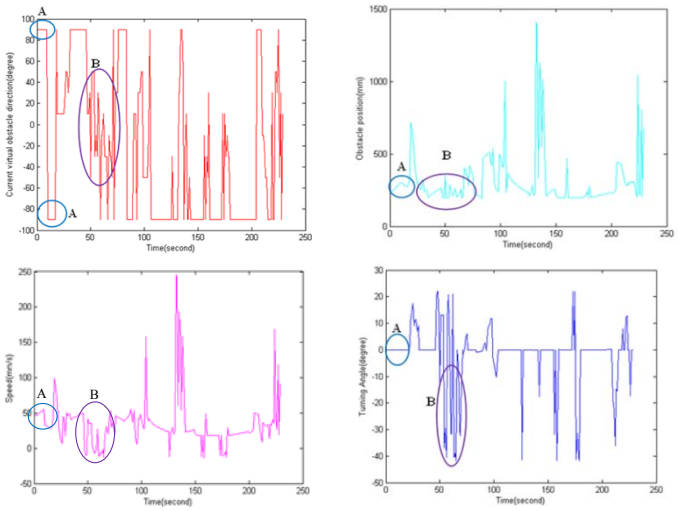

Figure 20. (Top Left) Current obstacle orientation w.r.t. the robot; (Top Right) Obstacle position; (Bottom Left) Velocity of the robot; (Bottom Right) Turning angle of the robot.

In region A, the robot detected an obstacle whose orientation changed between 90° and -90°. It indicates that the obstacle is at the right and the left side of the robot. The distance between the robot and the obstacles is about 250 mm. Hence, the robot maintained a slow speed of about 50mm/s without changing the heading angle.

In region B, the robot detected an obstacle whose orientation changed between 30° to -30°. It indicates that the obstacle is in front of the robot. The distance between the robot and obstacles so about 250 mm. The robot maintained a slow speed of about 25 mm/s. The robot continued to turn right until it is completely out of the dead zone of the U shape.

C. *Behavior of the integrated system*

First, the ANN classifies the current environment status of the robot and select corresponding FLC. Figure 21 shows the setup scenario of the robot.

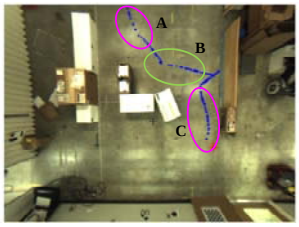

Figure 21. Setup scenario of the robot.

Figure 22 (Top Left) shows the trajectory of the robot from the starting point *S* (-513 mm, -2344 mm) to the target position *T* (1200 mm, 500 mm). The final position of the robot is (1062 mm, 346 mm). Figure 22 (Top Right) shows the distance between the robot and the target. The final distance error is 207 mm. Figure 22 (Bottom Left) and (Bottom Right) shows the velocity and the turning angle of the robot.

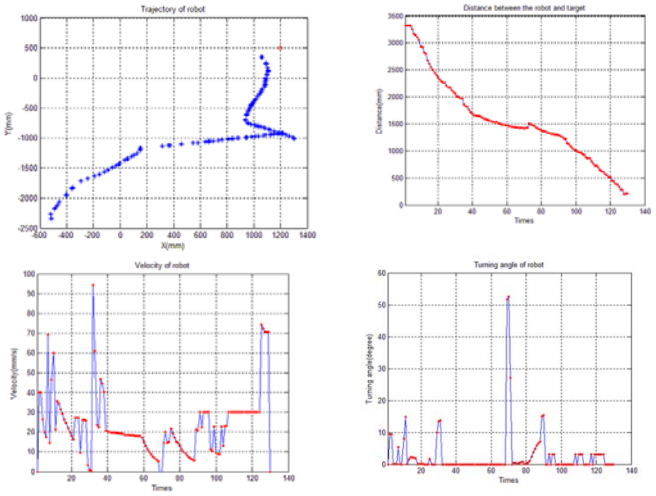

Figure 22. (Top Left) Trajectory of the robot; (Top Right) Distance between the robot and the target; (Bottom Left) Velocity of the robot; (Bottom Right) Turning angle of the robot.

Region A is classified as right-wall and the target position at left front. The target steering behavior is activated to navigate the robot to the target position. Region B is classified as the maze and the target position at right. It activated the obstacle avoidance behavior is activated to move the robot away from the obstacles. Region C is classified as left-wall and the target position at front. The target steering behavior is activated to move the robot to approach the target position.

D. *Micro-spectrometer-based content inspection*

Five different solutions, which often appear in a home

environment, are chosen as the spectrum database. They are vitamin B solution, cola drink, soy sauce, orange juice, and cough syrup. The spectra obtained from the micro-spectrometer for these specimens are shown in Figure 23.

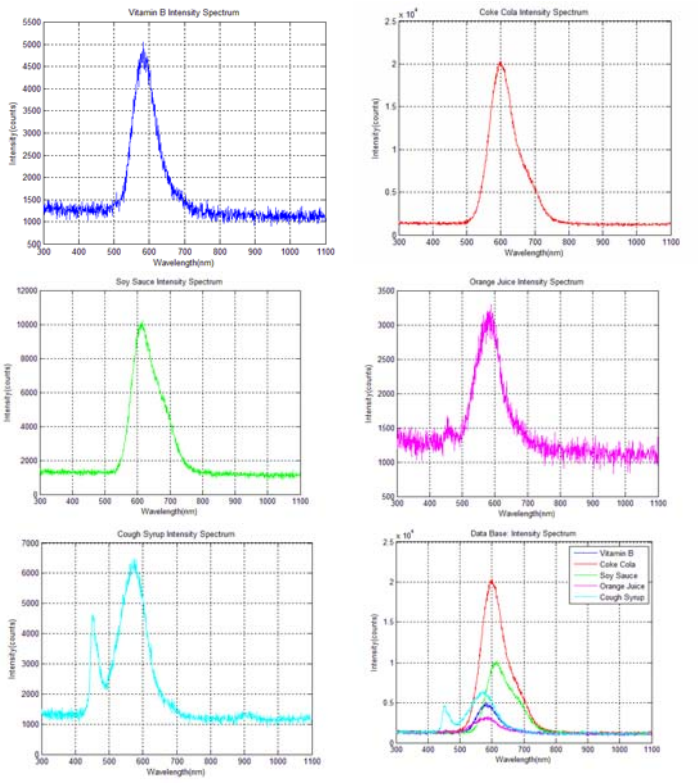

Figure 23. Intensity spectra of the database.

In order to compare with the tested content, the intensity spectra in the database are converted to transmittance and absorbance spectra, as shown in Figures 24 and 25, respectively.

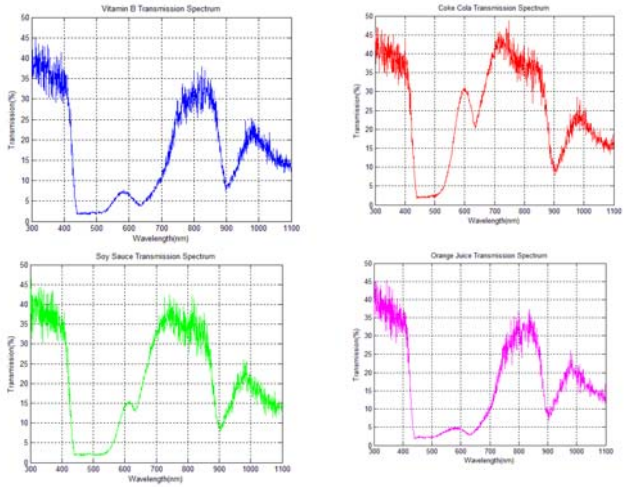

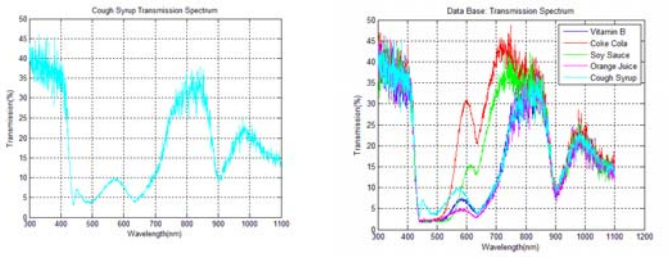

Figure 24. Transmittance spectra of the database.

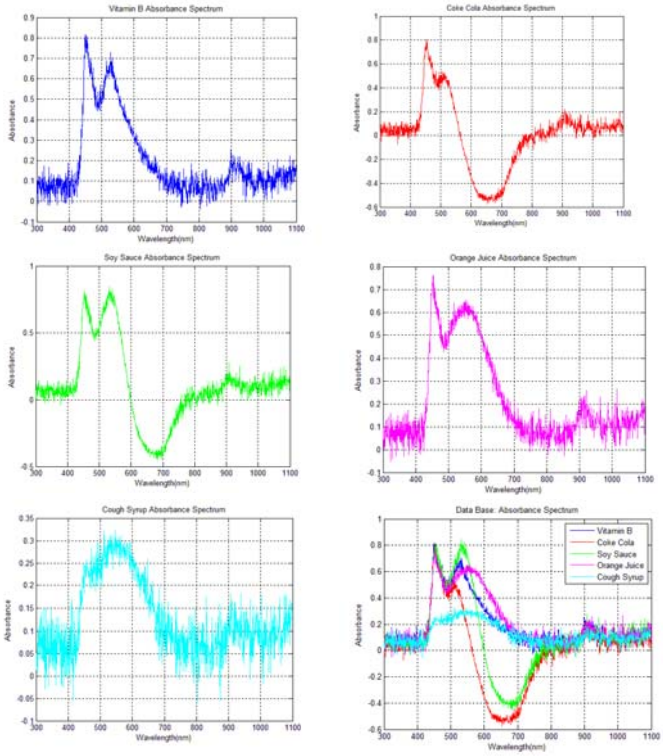

Figure 25. Absorbance spectra of the database.

Tables 15 through 17 present the similarity between the test spectra and the database spectra of both transmittance and absorbance, for different values of k. Table 15 shows that for $k = 0$, the absorbance result for cough syrup has a similarity level of 75%. For transmittance, the similarity is not satisfactory, the largest level of similarity being 20%, for both vitamin B and cough syrup.

Table 15. Similarity level at $k = 0$.

	Absorbance similarity	Transmittance similarity
Vitamin B	50%	20%
Cola	25%	0%
Soy sauce	25%	0%
Orange juice	50%	0%
Cough syrup	75%	20%

Table 16 shows that for $k = 5$, the absorbance result for cough syrup has a similarity level of 71.25%, which is smaller than the value for $k = 0$. For transmittance,

cough syrup gives a similarity level of 57%, which is bigger than that for $k = 0$.

Table 16. Similarity level at $k = 5$.

	Absorbance similarity	Transmittance similarity
Vitamin B	47.5%	38%
Cola	47.5%	0%
Soy sauce	23.75%	19%
Orange juice	47.5%	19%
Cough syrup	71.25%	57%

Table 17 shows that for $k = 10$, the absorbance result for cough syrup gives a similarity level of 67.5% which is smaller than the result for $k = 5$. For transmittance, cough syrup generates a similarity level of 54%, which is smaller than the value for $k = 5$.

Table 17. Similarity level at $k = 10$.

	Absorbance similarity	Transmittance similarity
Vitamin B	45%	36%
Cola	22.5%	0%
Soy sauce	22.5%	18%
Orange juice	45%	36%
Cough syrup	67.5%	54%

4. Conclusion

This paper presented the development and evaluation of a robot navigation system and micro-spectrometer-based content inspection device for homecare application. The navigation system controlled the motion of the mobile robot using an ANN as the situation classifier together with a FLC. The developed ANN demonstrated the ability to classify the robot's current environmental status. The results of the classifier determine which FLC should be activated. The developed FLC was successful in moving the robot to the target position while avoiding collisions.

The developed micro-spectrometer-based content inspection system compared histograms of the transmittance and absorbance spectra of the test specimens with spectra in the database. From examining the similarity, we can see that different k cause different similarity. Since that the content may have similar absorbance or transmittance spectrum, the combined examination can increase the identification rate which by calculate confidence level. The results showed that the proposed system possessed the ability to detect the unknown chemical contents for application in a robotic homecare system. In an actual home environment, this system is useful in identifying and administering prescribed medication.

References

[1] Secretary-General, "World demographic trends report," *United Nations - Economic and Social Council* 2009.

[2] "World report on disability estimate based on 2010 population," *World Health Organization and World Bank*, Geneva 2011.

[3] J. Schroeder, S. Wabnik, P. J. Hengel, and S. Goetze, "Detection and classification of acoustic events for in-home care," *Ambient Assisted Living*, R. Wichert and B. Eberhardt, Eds., Springer Berlin Heidelberg, pp. 181-195, 2011.

[4] J.-V. Lee, Y.-D. Chuah, and K. T. H. Chieng, "Smart elderly home monitoring system with an android phone," I*nternational Journal of Smart Home*, vol. 7, pp. 17-32, 2013.

[5] D. Kim, B. C. Min, and M.-S. Lee, "Fuzzy logic path planner and motion controller by evolutionary programming for mobile robots," *International Journal of Fuzzy Systems*, vol. 11, pp. 154-163, 2009.

[6] R. Baribeau, W. S. Neil, and É. Côté, "Development of a robot-based gonioreflectometer for spectral BRDF measurement," *Journal of Modern Optics*, vol. 56, pp. 1497-1503, 2009.

[7] J. A. Hilder, N. D. L. Owens, M. J. Neal, P. J. Hickey, S. N. Cairns, and D. P. A. Kilgour, "Chemical detection using the receptor density algorithm," *IEEE Trans. on Systems, Man, and Cybernetics, Part C: Applications and Reviews*, vol. 42, pp. 1730-1741, 2012.

[8] C. C. Tsai, C. C. Chen, C. K. Chan, and Y. Y. Li, "Behavior-based navigation using heuristic fuzzy kohonen clustering network for mobile service robots," *International Journal of Fuzzy Systems*, vol. 12, pp. 25-32, 2010.

[9] C.-H. Ko and M.-F. R. Lee, "Design and fabrication of micro-spectrometer based on silicon concave micro-grating," *Optical Engineering*, vol. 50, pp. 1-10, 2011.

[10] A. Das, D. Popa, J. Sin, and H. Stephanou, "Precision alignment and assembly of a Fourier transform microspectrometer," *Journal of Micro-Nano Mechatronics*, vol. 5, pp. 15-28, 2009.

[11] X. Li and B.-J. Choi, "Design of obstacle avoidance system for mobile robot using fuzzy logic systems," *International Journal of Smart Home*, vol. 7, pp. 321-328, 2013.

[12] C. Chen and P. Richardson, "Mobile robot obstacle avoidance using short memory: A dynamic recurrent neuro-fuzzy approach," *Transactions of the Institute of Measurement and Control*, vol. 34, pp. 148-164, 2012.

[13] K. Qian, A. Song, H. Zhang, and P. Xiong, "Path planning for mobile robot based on adaptive fuzzy neural network," *Dongnan Daxue Xuebao (Ziran Kexue Ban)/Journal of Southeast University (Nat-*

ural Science Edition), vol. 42, pp. 637-642, 2012.
[14] M. S. Guzel and R. Bicker, "A behaviour-based architecture for mapless navigation using vision," *International Journal of Advanced Robotic Systems*, vol. 9, 2012.
[15] S. Parasuraman and S. C. Yun, "Mobile robot navigation: Neural Q-learning," *International Journal of Computer Applications in Technology*, vol. 44, pp. 303-311, 2012.
[16] Y. Zhang, "Tracking control for wheeled mobile robots using neural network model algorithm control," *Journal of Theoretical and Applied Information Technology*, vol. 46, pp. 794-799, 2012.
[17] K.-H. Chi and M. R. Lee, "Obstacle avoidance in mobile robot using neural network," in *2011 International Conference on Consumer Electronics, Communications and Networks (CECNet)*, 2011, pp. 5082-5085.
[18] C.-H. L. Chen and M.-F. R. Lee, "Global path planning in mobile robot using omnidirectional camera," *2011 International Conference on Consumer Electronics, Communications and Networks, CECNet 2011*, Xian-Ning, China, 2011.
[19] M.-F. R. Lee and K. H.-E. Lee, "Autonomous target tracking and following mobile robot," *Journal of the Chinese Institute of Engineers, Transactions of the Chinese Institute of Engineers, Series A/Chung-kuo Kung Ch'eng Hsuch K'an*, vol. 36, pp. 502-529, 2013.
[20] T.-H. S. Li, M.-Y. Hsiao, and C.-Y. Chen, "Interval type-2 adaptive fuzzy sliding-mode dynamic control design for wheeled mobile robots," *International Journal of Fuzzy Systems*, vol. 10, pp. 268-275, 2008.
[21] Y.-C. Yeh, T.-H. S. Li, and C.-Y. Chen, "Adaptive fuzzy sliding-mode control of dynamic model based car-like mobile robot," *International Journal of Fuzzy Systems*, vol. 11, pp. 272-286, 2009.
[22] C.-C. Wong, C.-T. Cheng, K.-H. Huang, and Y.-T. Yang, "Fuzzy control of humanoid robot for obstacle avoidance," I*nternational Journal of Fuzzy Systems*, vol. 10, pp. 1-10, 2008.
[23] F. O. Karray and C. W. de Silva, S*oft Computing and Intelligent Systems Design: Theory, Tools, and Applications*, Pearson/Addison Wesley, 2004.

Min-Fan Ricky Lee is currently an Assistant Professor at the Graduate Institute of Automation and Control, National Taiwan University of Science and Technology, Republic of China (Taiwan). He received his Ph.D. (1996) and Master (1991) from Cornell University, USA. He was the Research Officer at the National Research Council in Federal Government of Canada (1998-2007) and the Research Scientist in University of British Columbia, Canada (1996 - 1998). His other professional service includes the member of Grant selection committee at the Natural Sciences and Engineering Research Council Canada (2005-2006) and Chair in IEEE Canada-Vancouver Section (2000-2001). He received the Outstanding Service Award from IEEE Canada.

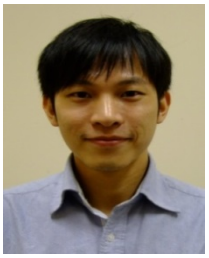

Fu-Hsin Steven Chiu is currently a Ph.D. Candidate at the Autonomous Mobile Robot Laboratory, National Taiwan University of Science and Technology. He received his MSc degree (2009) from Graduate Institute of Automation and Control, NTUST, Taiwan. His research areas are autonomous mobile robot, artificial intelligence and swarm intelligence, multi-robot systems. He has published papers on mobile robotics, fuzzy control system, networked predicts control,

Clarence W. de Silva is a Professor of Mechanical Engineering and occupies the Tier 1 Canada Research Chair Professorship in Mechatronics & Industrial Automation at the University of British Columbia, Vancouver, Canada. A Professional Engineer (P.Eng.), he is also a Fellow of: ASME, IEEE, Canadian Academy of Engineering, and the Royal Society of Canada. He has served as Editor/Associate Editor of 14 journals including ASME and IEEE transactions; and as Editor-in-Chief of International Journal of Control and Intelligent Systems.

Chia-Yu Amy Shih received the B.S. degree in department of Electrical Engineering, National Taiwan Ocean University in 2010. Her research interests include Autonomous mobile robot, navigation, ANN, FLC, micro-spectrometer, home care robotic system.